LAMELLAR NANOSTRUCTURE IN 'SOMASIF'-BASED ORGANOCLAYS

MIKHAIL Y. GELFER[1], CHRISTIAN BURGER[1], PRANAV NAWANI[1], BENJAMIN S. HSIAO[1,*], BENJAMIN CHU[1], MAYU SI[2], MIRIAM RAFAILOVICH[2], GRAZYNA PANEK[3], GUNNAR JESCHKE[3], ALEXANDER Y. FADEEV[4] AND JEFFREY W. GILMAN[5]

[1] Chemistry Department, Stony Brook University, Stony Brook, NY 11794, USA
[2] Materials Science and Engineering Department, Stony Brook University, Stony Brook, NY 11794, USA
[3] Max-Planck Institute for Polymer Research, Postfach 3148, 55021 Mainz, Germany
[4] Chemistry Department, Seton Hall University, 800 South Orange Avenue, South Orange, NJ 07009, USA
[5] Fire Research Division, National Institute of Standards and Technology, Gaithersburg, MD 20899-8665, USA

Abstract—Thermally induced lamellar structure changes due to phase transition and degradation in organoclays based on a synthetic 'Somasif' mineral and two organic surfactants, di-methyl dihydro-di-tallow ammonia chloride (DMDTA) and tri-butyl-hexadecyl phosphonium bromide (HTBP) were investigated by differential scanning calorimetry (DSC), thermogravimetric analysis (TGA), Fourier transform infrared (FTIR) spectroscopy, *in situ* simultaneous small-angle X-ray scattering (SAXS) and wide-angle X-ray diffraction (WAXD) over the temperature range 30−280ºC. Results indicated that the surfactant layer in 'Somasif'-based organoclays underwent thermally induced melting-like order-disorder transition followed by desorption of surfactant molecules, resulting in drastic changes in the character of the layer periodicity. The transition temperature (T_{tr}), determined from the endothermic transition in DSC, was found to depend strongly on the type and the content of surfactant incorporated. Temperature-resolved SAXS indicated complex intercalated layered structures, containing multiple lamellar stack populations of two different organic layer thicknesses. A weak scattering peak (s_0), located at exactly the half angular position of the strong first scattering maximum s_1 ($s_0 = 0.5s_1$), was found in all tested 'Somasif' clays. The presence of this peak can be attributed to a slight breaking of the translational symmetry in the layered structure, causing the 1D repeat period in real space to be doubled. In other words, some portions of layers are grouped into pairs and a single pair forms the new repeat unit. This arrangement is reminiscent of the Peierls-like distortion.

Key Words—Degradation, Organoclays, 'Somasif', Surfactant, Thermal Transition, SAXS.

INTRODUCTION

The intercalated organoclays formed by electrostatic interactions between layer silicates and surfactants have long been an active research subject in the mineralogy community (Walker, 1967; Johns and Sen Gupta, 1967; Malik *et al.*, 1972; Lagaly *et al.*, 1975; Lagaly, 1986; Ijdo and Pinnavaia, 1998, 1999). In recent years, the interest in organoclays has also been expanded into the polymer community. A broad variety of organoclays has been synthesized and characterized with the aim of preparing new polymer composites (Vaia *et al.*, 1994; Hackett *et al.*, 1998; Lee *et al.*, 2000; Xie *et al.*, 2001). It has been shown that the surfactant component can promote the exfoliation of layer silicates in the polymer matrix and create a 'nanocomposite', which can result in superior thermal stability, barrier and mechanical properties when compared to the unfilled polymer matrix (Krishnamoorti *et al.*, 1996; Vaia and Giannelis, 1997; LeBaron *et al.*, 1999; Alexandre and Dubois, 2000). The extent of clay exfoliation often depends on the dispersion method used. The method of melt mixing is the most practical way to

compound polymer nanocomposites. However, the dispersion of organoclay by melt mixing may be limited because of the likelihood of thermal degradation and desorption of the organic component in organoclay (Gelfer *et al.*, 2005). In this study, the issue of thermal stability in a new kind of 'Somasif' organoclay has been investigated. As melt mixing is always performed at elevated temperatures (*e.g.* >150ºC), the relatively low thermal stability of the surfactant component in organoclays can be a major problem. Understanding the thermally induced structural changes in this organoclay can enable us to improve the control of clay dispersion in the polymer matrix *via* melt mixing.

In a previous study (Gelfer *et al.*, 2004), we described the temperature dependence of structure change in organoclays based on 'Cloisite', a product produced by processing a naturally occurring montmorillonitic material. 'Cloisite'-based organoclays have been the popular choice for academic research as well as commercial applications. However, as research and applications of organoclays grow, the disadvantages of using 'Cloisite'-based organoclays also become more obvious. The shortcomings of 'Cloisite'-based organoclays include the structural heterogeneity (Krishnamoorti *et al.*, 1996; Vaia and Giannelis, 1997; Hackett *et al.*, 1998; LeBaron *et al.*, 1999; Lee *et al.*, 2000; Alexandre and Dubois,

140

2000; Gelfer *et al.*, 2004) and the presence of various impurities (*e.g.* transition metal ions (TMI)). The structural heterogeneity in 'Cloisites' due to the variation of chemical constituents often causes discrepancy in ion exchange capacity between different layers, which can result in complicated characteristics of intercalation in corresponding layered structures. Impurities can lead to undesired colors as well as catalytic activity, which can result in degradation of the surfactant at elevated temperatures during melt processing.

It may be because of these reasons that new synthetic clays such as 'Somasif' have started to attract a great deal of attention for the preparation of organoclays and nanocomposites. 'Somasif' is a synthetic, smectite-like clay (Tateyama *et al.*, 1992). It is expected to have a very low TMI content. In contrast to 'Cloisite', 'Somasif' does not contain catalytically active Al ions in the octahedral sheets within the mineral layers. This may lead to greater thermal stability of the organic component in corresponding organoclays or/and polymer nanocomposites when compared to the 'Cloisite'-based system. There has been no previous systematic investigation of the thermal behavior and temperature dependence of structural changes in 'Somasif'-based organoclays, hence this study.

We utilized a variety of experimental techniques including differential scanning calorimetry, thermogravimetric analysis, Fourier transform infrared spectroscopy, scanning electron microscopy, small-angle X-ray scattering, wide-angle X-ray diffraction and analytical SAXS modeling techniques to examine the thermal transition and corresponding structural changes in a series of organoclays based on 'Somasif' clay (SME100) and two types of surfactants. Similar to our previous study (Gelfer *et al.*, 2005), the emphasis of this work also included the development of a reliable scheme to interpret the SAXS results from the SME100-based layered silicates. The rationale for the modeling effort is as follows. The large density difference between the mineral silicate and the organic component in organoclays has made SAXS a natural technique to characterize the structures of organoclays (Johns and Sen Gupta, 1967; Malik *et al.*, 1972; Lee *et al.*, 2000; Xie *et al.*, 2001). It has been shown that the degree of delamination between layered silicates and the distribution of interlayer distance in organoclays can be determined from SAXS (Reynolds, 1980; Tateyama *et al.*, 1992). This information is particularly useful for the analysis of nanocomposites because one can study the affinity between the polymer chains and the organoclays based on changes in the SAXS profiles from organoclays to composites (Giannelis *et al.*, 1999; Alexandre and Dubois, 2000). For example, the shift of the first scattering maximum towards a lower scattering angle can be attributed to the increase of the interlayer distance, caused by intercalation of organoclay stacks through polymer penetration; while the broadening of

the scattering peak and the decrease of the scattering intensity can be attributed to an increase in the degree of stacking disorder (Gelfer *et al.*, 2004).

However, if one wishes to determine the state of intercalation and exfoliation in organoclays quantitatively from the SAXS data, the task becomes much more difficult. This is because there are many factors, including the defects in organic-layered silicate complexes, heterogeneous distribution of interlayer periodicity, difference in packing density of the organic component, interstratification of different arrangements, and variation in distribution of alkyl chain length of surfactant used, all of which can lead to the broadening or/and shifting of scattering peaks (Jonas and Grim, 1957; Giannelis *et al.*, 1999). In our previous work (Gelfer *et al.*, 2004), we showed that in 'Cloisite'-based organoclays, the presence of heterogeneous interlayer thickness distribution (*i.e.* interstratification) can cause significant deviation in the location of scattering peak from the expected value based on Bragg's law. This problem has been highlighted before (Reynolds, 1980; Brindley and Brown, 1980). In addition, thermal degradation of 'Cloisite'-based organoclays could cause weakening or even complete disappearance of scattering signals (Gelfer *et al.*, 2004); the presence of surface defects in organic-layered silicate complexes and the breaking of clay stacks from the surfactant treatment, although relatively minor compared to the effect of interstratification, could also result in signal broadening (Hosemann and Bagchi, 1962; Alexander, 1969; Reynolds, 1980). In this study, we applied and expanded our previously developed procedures (Gelfer *et al.*, 2004) for quantitative analysis of the SAXS data from the 'Somasif'-based organoclays. The unique analytical schemes allowed us to account for the interlayer thickness distribution within the organoclay stacks as well as the correlation between the thicknesses of neighboring layers. We assumed that the effects due to the surface defects in 'Somasif'-based organoclays are negligible.

MATERIALS AND METHODS

Samples and preparation

The 'Somasif' sample (SME100) chosen is a synthetic clay mineral manufactured by Unico (Japan) using an undisclosed solution-precipitation process followed by a high-T thermal treatment. According to the manufacturer, 'Somasif' has a general chemical composition of $(Na)_{2x}(Mg)_{3-x}(Si_4O_{10})(F_aOH_{1-a})_2 \cdot nH_2O$, where $0.15 < x < 0.5$; $0.8 < a < 1.0$. SME100 is a smectite-like mineral, similar to naturally occurring montmorillonitic materials, such as 'Cloisite'. However, in contrast to montmorillonite (montmorillonite's general composition is $(Na_y)(Al_{2-y}Mg_y)(Si_4O_{10})(OH)_2 \cdot nH_2O$; $0.25 < y < 0.6$), 'Somasif' does not contain catalytically active Al ions as a substitute in octahedral positions within the mineral

layers. Another difference is its partial substitution of hydroxyl groups within the silicate layers with fluorine. It is known that 'Cloisite' materials can undergo dehydroxylation above 600ºC (Jonas and Grim, 1957), losing apical OH groups and transforming into an anhydrite form. Obviously, the dehydroxylation process will be hindered in a fluorinated 'Somasif' mineral.

Several 'Somasif' organoclay samples were chosen: (1) 'Somasif'-MAE (SMAE), manufactured by Co-Op Chemical Co., Japan, contained 'Somasif' SME100 mineral and di-methyl-di-hydrogenated-talloammonium chloride (DMDTA) surfactant (42 wt.%). DMDTA was a blend of surfactants prepared from natural products by Akzo Nobel. According to Akzo Nobel, the major component in this blend was dimethyldioctadecyl ammonia chloride (DMDOA); minor components included (in the order of decreasing content) dimethyl-octadecylhexadecyl ammonia chloride, dimethyldihex-adecyl ammonia chloride and a small (<3 wt.%) amount of tertiary ammonia chlorides (such as dimethyloctade-cyl ammonia chloride and dimethylhexadecyl ammonia chloride). (2) 'Somasif'-P organoclays, made by Panek and Jeschke from the Max Planck Institute for Polymer Research, contained 'Somasif' ME100 and tributylhex-adecylphosphonium bromide (HTBP) (Aldrich). The preparation schemes for 'Somasif'-P organoclays will be described elsewhere. 'Somasif'-P organoclays con-tained ~25 wt.% of HTBP which was used in two forms (a) the as-synthesized form (SomP), and (b) the ther-mally annealed form (SomPan). The latter was prepared in order to explore the effect of thermal annealing on the clay morphology. SomPan was prepared by holding the organoclay at a temperature of 160ºC for 30 min in a heat press model PW (P.O. Weber Maschinen und Apparatebau GmbH, Remshalden, Germany) at 70 MPa in air, and subsequently quenched to room temperature. These conditions are the same as for polymer-clay nanocomposites prepared in a related work (Panek *et al.*, 2006). No surfactant loss was detected under these conditions. Samples for all tests were prepared by compressing powders into pellets (1−2 mm thick) which were isotropic and did not possess preferred orientation, verified by both SAXS and WAXD evalua-tions (data not shown).

Characterization techniques

Differential scanning calorimetry heating and cooling patterns were measured at a rate of 10ºC/min in a nitrogen environment using a Mettler Model 821e device (Mettler, Toledo). A cyclic thermal protocol, including heating from 5 to 180ºC with subsequent cooling back to 5ºC, was used. Thermogravimetric analysis measure-ments were performed using a TGA 2950 device (TA Instruments). Measurements were carried out in nitro-gen. The thermal protocol applied in TGA measurements included heating at a constant rate of 10ºC/min from 30 to 900ºC.

Simultaneous SAXS and WAXD measurements were carried out at the X27C beamline in the National Synchrotron Light Source (NSLS), Brookhaven National laboratory (BNL). The X-ray wavelength used was 0.1366 nm, collimated by a three-pinhole collimation system. A dual-chamber temperature jump apparatus (Chu and Hsiao, 2001), which could hold the experimental tem-perature with an accuracy of ± 1ºC, was used. The experiment was performed using a stepped temperature protocol. The sample was held isothermally at the experimental temperature for 3 min and then rapidly (>30ºC/min) brought to the next experimental tempera-ture. The experimental setup used in SAXS experiments allowed for a rapid temperature equilibration.

The SAXS/WAXD 2D images were acquired using two image plates (Fuji Company). 1D scattering/diffraction profiles were obtained by integrating 2D images using the Polar software developed at Stonybrook Technology and Applied Research (Stony Brook, NY). The sample-to-detector distances for SAXS was 840 mm and for WAXD was 130 mm. The scattering angle in SAXS was calibrated by a silver behenate standard and the diffraction angle in WAXD was calibrated by an Al_2O_3 standard from the National Institute of Standards and Technology. All scattering/diffraction signals were corrected for beam fluctuations, sample absorption and background scattering.

Fourier transform infrared measurements were per-formed with a Spectrum One FTIR device (Perkin Elmer) using a MCT (mercury cadmium tellurium) detector. The data were collected in reflection mode using the Harrick Seagull accessory (Harrick, Ossining, NY), where the spectra were taken at a 45º angle of the incidence beam. In total, 100 scans with a resolution of 4 cm^{-1} were recorded. Spectra at high temperatures were collected using the IR High Temperature Reaction Chamber (Harrick).

Scanning electron microscopy images of unmodified 'Somasif' clay and organoclays were obtained using a JSU-5300, Jeol SEM microscope. All clay samples were finely powdered and sputter coated with gold. The SEM images were taken at various magnifications using a back-scattering detector.

RESULTS AND DISCUSSION

'Somasif'-based organoclays were characterized by SEM. The results showed that all chosen 'Somasif' unmodified clay and modified organoclays exhibited a significant amount of needle-like tubular structures along with clay platelets (a typical SEM image of SME100 with tubular structure is shown in Figure 1). These tubules were 200−300 nm in diameter and 3−10 μm long. We hypothesize that the tubular struc-tures may be formed as a by-product of the SME100 synthesis and can be considered as the synthetic analogs of naturally occurring tubular chrysotile minerals
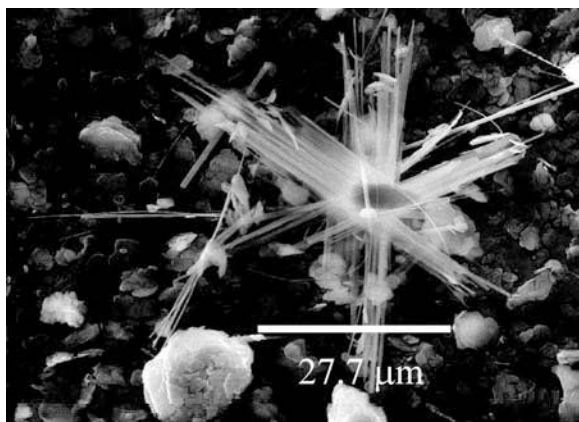
Figure 1. Typical SEM image of the synthetic 'Somasif' mineral (SME100).

($Mg_3Si_2O_5(OH)_4$) (Brindley and Brown, 1980). The possible structure of tubular inclusions will be discussed in more detail later. Below, we will first describe the thermal stability results (by TGA and DSC), followed by the FTIR data, temperature-dependent SAXS/WAXD data, and the structure analysis based on the SAXS data.

Thermal analysis

Figure 2 shows TGA patterns of selected unmodified clay (SME100), modified organoclays (SMEA, SomP and SomPan) and corresponding surfactants (DMDTA and HTBP). It is interesting to note that SME100 did not undergo structural dehydroxylation above 600ºC, in contrast to 'Cloisite'. The observed high-T stability in SME100 may be attributed to the substitution of hydroxyl groups for fluorine. In the case of organoclays, the order of thermal stability is SomP $\approx$ SomPan > SMAE. The greater thermal stability of SomP organoclays compared to that of SMAE organoclays is probably related to the greater thermal stability of HTBP surfactant as compared to DMDHTA (Figure 2).

The DSC thermograms of selected 'Somasif'-based organoclays (SMAE, SomP and SomPan) and the corresponding surfactant (HTBP) are shown in Figure 3. All tested organoclays (SomP a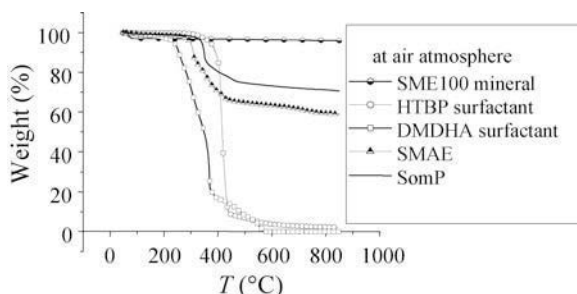nd SMAE) exhibited a major endothermic peak at temperatures close to the melting peak of the corresponding surfactant. This suggests that the surfactant phase in organoclays was at least in an ordered state (*e.g.* liquid crystal or pseudo-crystal) and could undergo a melting-like transition upon heating. For SMAE, the transition temperature ($T_{tr} = 35$ºC) determined from the endothermic peak position in DSC was significantly lower than the melting temperature of the DMDHTA surfactant ($T_m = 70$ºC). On the other hand, the transition temperature in SomP ($T_{tr} = 66$ºC) was slightly higher than the melting temperature of HTBP ($T_m = 62$ºC). In Figure 3, a small but distinct endothermic peak was observed at 160ºC for both the SomP and SomPan samples (also SME100 and SMAE). However, this peak was absent in thoroughly dried samples or in the second heating cycle. This implies that the peak may be related to desorption of strongly bound water. We hypothesize that the bound water may be attached to the cationic head-group of the organic component in SomP or SMAE organoclays. The water adsorption phenomenon was also consistent with the appearance of small endothermic peak at 0ºC (*i.e.* melting of ice crystals) in DSC (Figure 3) and the small weight loss in the region of 140−200ºC for all 'Somasif' samples (Figure 2). From these data, we conclude that the chosen annealing treatment (*i.e.* holding the sample at a temperature of 433 K for 30 min at 70 MPa) does not change the structure or thermal properties of SomP.

Structure characterization by FTIR

Fourier transform infrared spectroscopy is a useful tool for characterizing the conformational change in the surfactant layer in organoclays. This is because the surfactant component contains long alkyl chains, where the frequencies of CH_2-stretching bands (2800−3000 cm^{-1}) can reflect the state of conformational order in the adsorbed organic layers (Hair, 1967; Snyder *et al.*, 1982; Porter *et al.*, 1987; Parikh *et al.*, 1995; Kojo *et al.*, 1998). For a completely disordered structure, such as liquid alkanes, the characteristic frequencies are 2924 cm^{-1} for CH_2 symmetric stretching

Figure 2. TGA graphs of the 'Somasif' clay, organoclays and corresponding surfactants (heating rate of 10ºC/min).
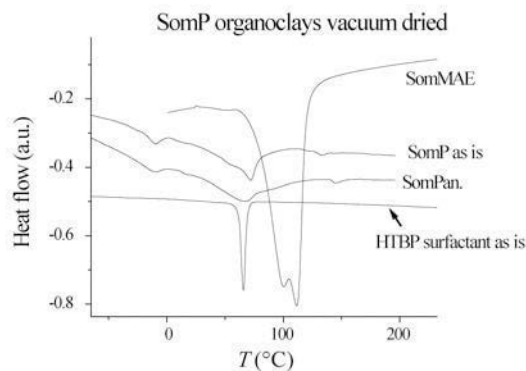

Figure 3. DSC graphs of selected 'Somasif'-based organoclays (SomP and SomPan) and the corresponding surfactant (HTBP) (heating rate of 10ºC/min).
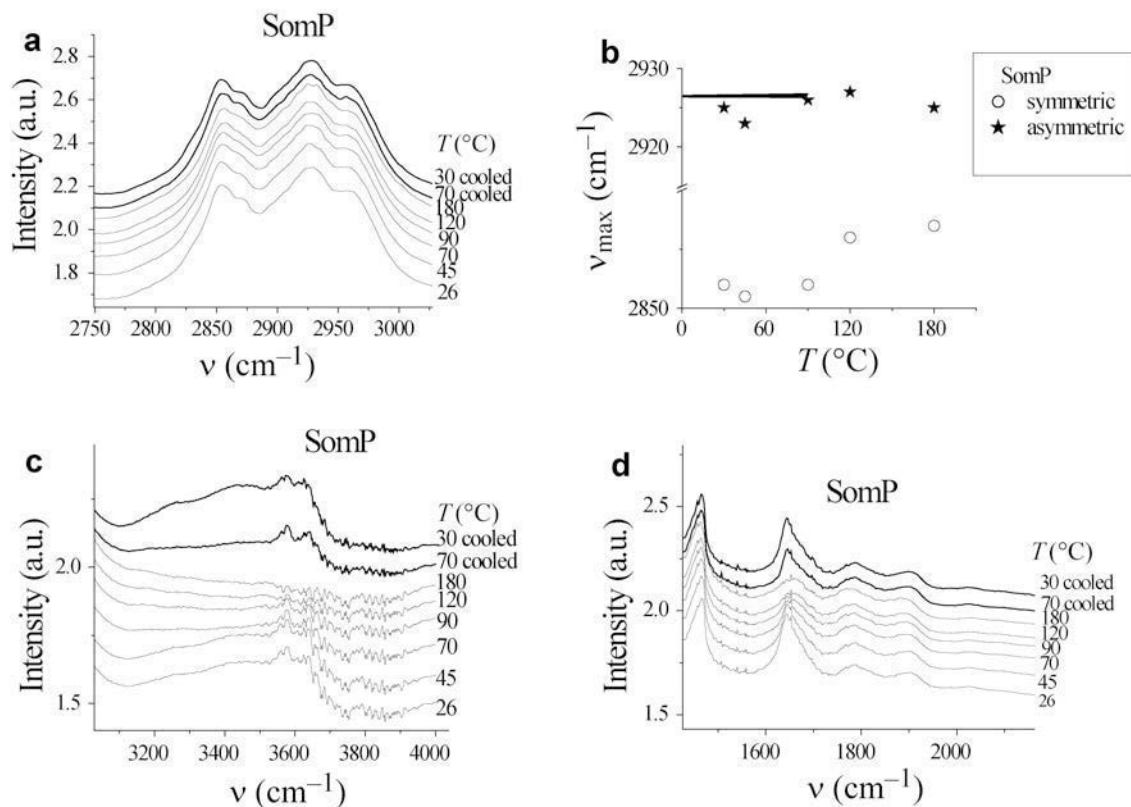
Figure 4. (a) Typical FTIR spectra for SomP collected between 2800 and 3000 cm^{-1}; (b) changes in the corresponding CH$_2$-stretching frequencies; (c) the spectra showing the change in the band at 3600 cm^{-1} (OH stretching) with temperature, (d) the spectra showing the change in the band at 1650 cm^{-1} with temperature.

and 2856 cm^{-1} for CH$_2$ asymmetric stretching. For well-ordered layers, such as crystalline paraffin in all-*trans* conformation, the characteristic frequencies are 2915–2918 cm^{-1} for CH$_2$ symmetric stretching and 2846–2850 cm^{-1} for CH$_2$ asymmetric stretching.

The typical FTIR spectra for SomP collected between 2800 and 3000 cm^{-1} are shown in Figure 4a, and the corresponding peak positions of CH$_2$ symmetric stretching and asymmetric stretching for both SMAE and SomP at varying temperatures are shown in Figures 4b. In Figures 4b, it is seen that the CH$_2$-stretching frequencies in SomP are very close to those in liquid alkanes. This suggests that the organic layers in SomP do not have a significant degree of order. However, we observed partial ordering in the surfactant layers of SMAE at 30ºC (data not shown, but ν_{max} = 2920 cm^{-1} for CH$_2$ symmetric stretching; 2851 cm^{-1} for CH$_2$ asymmetric stretching were seen) and the system became disordered upon heating to 50ºC. The lower *trans*-content observed in SomP than SMAE should not come as a surprise. This is because the bulky tri-butyl phosphonium head-group would hinder the dense packing of hexadecyl tails. Based on the presence of a melting-like transition in DSC traces, we suggest that all tested 'Somasif' organoclays possess partial ordering, which was also

seen in our previous study of 'Cloisite'-based organoclays (Gelfer *et al.*, 2004).

The FTIR results indicate that the temperature dependence of the chain conformation in the surfactant layer was more pronounced in SMAE than SomP. This may be partially due to the fact that in SomP, the vibration signals from nine CH$_2$ segments in three butyl groups from the HTBP surfactant can contribute to the intensity of the CH$_2$ band in the FTIR spectrum. As the butyl groups are in the disordered conformation state at low temperatures (*e.g.* 30ºC), the temperature dependence of ν_{max} for butyl methylenes is rather weak. On the other hand, in SMAE, the dense packing of hydrocarbon tails in the surfactant can lead to the crystallization of alkyl chains, whereby the melting-like order-disorder transition can occur during heating.

It was suggested in the literature that in contrast to clay minerals, organoclays are hydrophobic, making them compatible with hydrophobic polymers (Alexandre and Dubois, 2000). However, our FTIR data suggest that even at the high surfactant loading (*e.g.* 30 wt.% in SomP), 'Somasif'-based organoclays seem to exhibit a tendency to absorb water. This is because distinct O−H stretching signals, which appeared as a doublet at ~3567 and ~3630 cm^{-1}, were observed in Figure 4c. These

peaks could be attributed to the water (H−O−H) stretching or magnesium hydroxide (Mg−O−H) stretching signals. Since the peaks were distinct at temperatures below 100ºC but decreased in intensity with temperature (they disappeared above 120ºC), we argue that they are mainly due to the motion of water stretching. In addition, the signals disappeared upon heating but recovered upon cooling (in air), suggesting that reversible adsorption and desorption of water took place. This behavior was also observed in the intensity change of the 1650 cm^{-1} band (Farmer, 1974). The 1650 cm^{-1} band could be related to the water bound to interlayer cations, which decreased notably at temperatures above 100ºC and it recovered upon cooling (Figure 4d). A similar phenomenon was previously reported in 'Cloisite'-based organoclays (Lagaly *et al.*, 1983; Lagaly, 1987; Moraru, 2001; Gates, 2004).

Temperature-resolved SAXS and WAXD studies

The SAXS profiles for both types of 'Somasif'-based organoclays (SomP and SMAE) show distinct scattering peaks (Figures 5a, 5b), which were very different from each other. They are also different from those observed in our previous study of 'Cloisite'-based organoclays (Gelfer *et al.*, 2004). At first sight, the scattering profiles for the two 'Somasif'-based organoclays appeared to be complex mixtures of different structures. However, an in-depth examination revealed some surprising insights into the structures and corresponding temperature

Figure 5. Temperature-resolved SAXS profiles for (a) SomP, and (b) SMAE organoclays.

dependences in these two systems. A simple structure model with very few parameters can fully account for all scattering features observed in both organoclays.

Before we discuss our modeling scheme in detail, some premises for the structure arrangement of organoclays are first outlined as follows. Organoclays are layer silicates intercalated with organic surfactants. The silicate layers can be considered rigid and inert in the temperature range of the experiment. Thus, we can assume that all observable structures have the form of lamellar stacks; whereby the SAXS treatment can be reduced to the scenario of 1D projection of the lamellar system onto its lamella normal (in the limit of sufficiently large lateral layer extensions). Furthermore, the silicate layers can be considered perfectly monodispersed (~1 nm thick) such that (1) all thickness variations of the lamellar system are generated by the organic layers, and (2) the scattering problem can be reduced to the structural factor corresponding to the centers of silicate layers.

In Figure 5, the most striking feature of all measured SAXS profiles is the presence of a weak scattering maximum (marked by an asterisk) at around one half (and also at three halves) of the position of the intense peak associated with the lamellar long spacing. Such a peak is located at $s = 0.2$ nm^{-1} for SomP and $s = 0.15$ nm^{-1} for SMAE. As the silicate layers are assumed to be rigid and inert (*i.e.* they do not undergo any conformational change, chemical transformation or density change), the most likely explanation for the occurrence of this peak is a small translational displacement of neighboring layers, leading to the formation of loosely coupled pairs. This structure is similar to the 'Peierls effect' in solid-state physics (of course, the origin of the classical Peierls effect is quite different from that observed here, but we still refer to the phenomenon in this study as 'Peierls-like' for its striking similarity). In other words, the presence of the above unique scattering peak indicates a breaking of translational symmetry and a doubling of the repeat period in the 1D structure, spanning two basal spacings.

A possible explanation for the Peierls-like lamellar structure is as follows: in a stack of organoclay, we assume that each silicate layer has two different surfaces, schematized as dark and light in Figure 6. The stack contains alternating surfaces so that light and light, and dark and dark surfaces, respectively, are facing each other. This alternating stack structure is intercalated by organic layers that, for reasons yet to be determined, preferably assume one of two possible discrete thicknesses. Figure 6 illustrates three possible arrangements for the stack. The stack with a single organic layer thickness possesses an equidistant period of either all long (AA type) or all short (BB type) long spacings, as illustrated in Figures 6a and 6c, respectively. If the stack possesses an alternating sequence of long and short organic layer thicknesses, we refer to it as
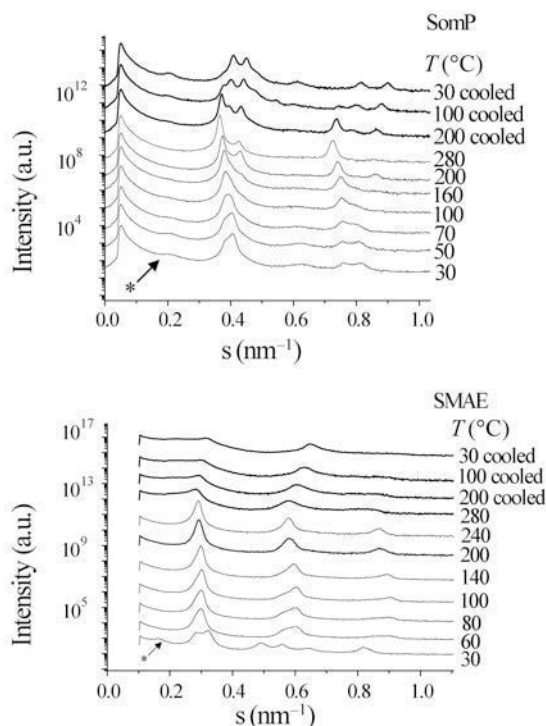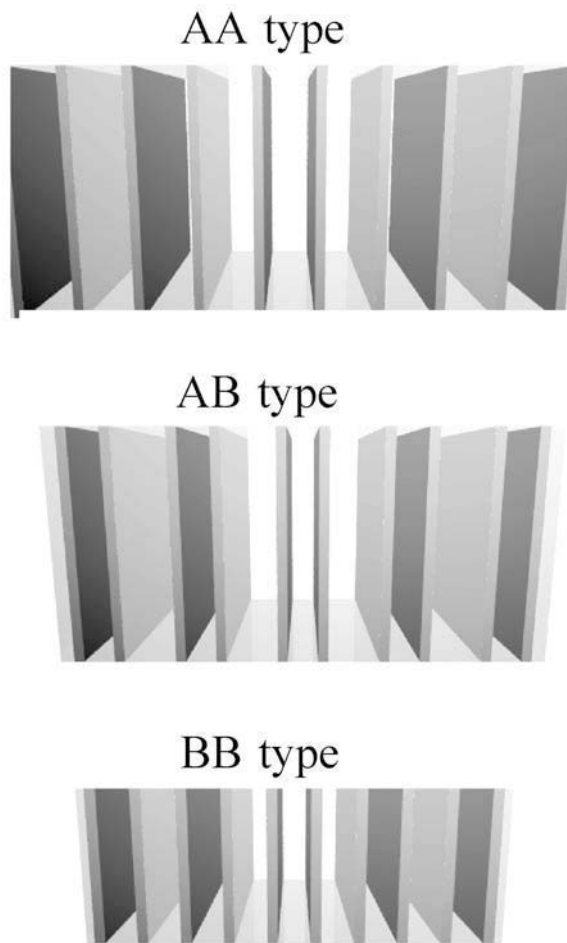
AA type

AB type

BB type

Figure 6. Schematic representation of the lamellar stacks having equidistant or alternating spacings: (a) equidistant lattice with large organic layer thickness (large long spacing); (b) Peierls-distorted lattice with alternating spacings (AB-like); (c) equidistant lattice with short organic layer thickness (short long spacing).

the Peierls-distorted stack with AB-type periodicity (Figure 6b).

Clearly, the stacks in Figure 6a (with the long organic layer thickness) and Figure 6c (with the short organic layer thickness) will produce scattering curves consisting only of equidistant peaks, the strongest of which will indicate the corresponding long spacing. Only the Peierls-distorted alternating stack in Figure 6b will generate a weak peak at one-half the position of the main basal peak. Examination of the experimental scattering curves in Figure 5 suggests the following scenario. At low temperatures before the heating cycle, the system consists of a mixture of equidistant stacks with the long organic layer thickness (AA-type periodicity) and Peierls-distorted alternating stacks. Increasing the temperature leads to a gradual disappearance of the Peierls-distorted stacks (and the corresponding Peierls peak) in favor of the equidistant stacks with the longer

long spacing, which also increases slightly during heating (*i.e.* the peak position shifts to a lower *s* value). In addition, a new set of equidistant peaks emerges at larger scattering angles, corresponding to the shorter long spacing. At the highest temperature of 280ºC, the system essentially consists of a mixture of equidistant stacks with either long or short long spacing but no additional Peierls component. Upon cooling, the original stacks with longer long spacing gradually disappear, while the new stacks with shorter long spacing (BB-type periodicity) persist and the Peierls-distorted alternating stacks are reconstituted. Thus, the final cooled-down product consists of a mixture of equidistant stacks with short long spacing and Peierls-distorted stacks.

To treat the scattering data from the alternating sequence in a Peierls-distorted stack quantitatively, we consider J.J. Hermans' original treatment (Alexander, 1969) of a 1D two-phase system in a stacking model

$$I_1(s) = (2\pi^2 s^2)^{-1} \mathrm{Re}\left[\frac{(1-H_1)(1-H_2)}{1-H_1H_2}\right] \qquad (1)$$

with independent statistics of neighboring interface distance distributions. These distributions can be given as Gaussian functions so that their Fourier transforms become

$$H_j(s) = \exp(2\pi i d_j s - 2\mathrm{p}^2\sigma_j s^2) \qquad (2)$$

where d_j represents the average layer thicknesses and σ_j represents the dispersion of the layer thickness distribution. For an ideal two-phase system, H_1 and H_2 are Fourier transforms of the thickness distributions of organic and mineral layers, respectively, and the 1D Porod law, $I_1 \approx s^{-2}$, should be obeyed. However, for the Peierls-distorted stack, we can modify the model as follows. The system can be considered as having a point lattice with H_1 and H_2 being Fourier transforms of the thickness distributions of two different organic layers and the mineral layer can be introduced *via* the form factor. We note that there is no Porod's law for the lattice factor. The calculation of the lattice factor for the Peierls-distorted point lattice thus involves essentially the same summable convolution polynomial series, apart from a few changes of signs and leads to a rather similar result as equation 1.

$$I_1(s) = \lim_{N \to \infty} \frac{1}{N} I_{1,N}(s) = (2\pi^2 s^2)^{-1} \mathrm{Re}\left[\frac{(1-H_1)(1-H_2)}{1-H_1H_2}\right]$$
$$(3)$$

In either case, the 3D powder-averaged scattered intensity profile can be obtained by

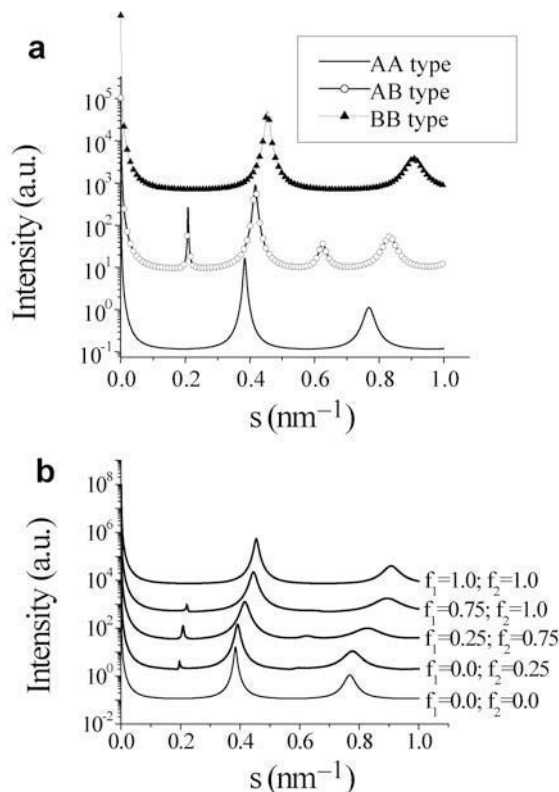$$I(s) = \langle I_1(s)\rangle_w = (2\pi s^2)^{-1} I_1(s) \qquad (4)$$

Figure 7. (a) Scattering curves corresponding to the three different stacks in Figure 6, calculated using equations 2−4, d_1 = 2.6 nm, d_2 = 2.3 nm, $\sigma_1 = \sigma_2 = 0.15$ nm. The equidistant long- and short-spaced stacks were obtained by appropriately setting $H_1 = H_2$. (b) The attenuation of the Peierls peaks by perturbation of the perfect alternation using the linear combination (equation 5) of distance distributions with parameters f_j as indicated

Figure 7a shows the calculated scattered intensity profiles corresponding to the models in Figure 6. As will be discussed below, the typical values used in the calculation are 1 nm for the monodispersed silicate layer thickness, 2.6 nm for the thicker organic layer thickness and 2.2 nm for thinner organic layer thickness. The additional peaks generated by the Peierls distortion are clearly visible but a little too strong and sharp. The
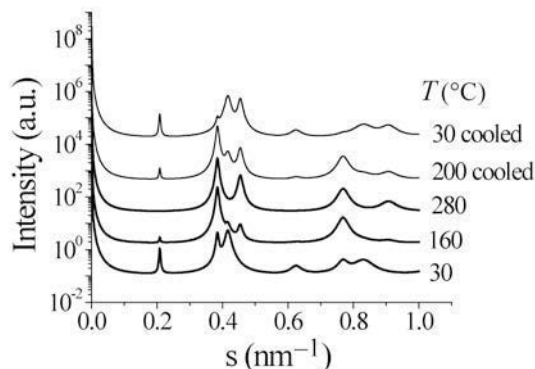

Figure 8. Attempt to reproduce selected experimental scattering profiles semi-quantitatively for SomP in Figure 5a. The calculation was performed by suitable combinations of the functions shown in Figure 7 using the modification of equation 5 with f_1 = 0.1 and f_2 = 0.9.

intensity of the Peierls peak will be decreased if the alternation of short and long layer thicknesses is not perfect, which can be modeled by replacing the original H_j in equation 3 by the following linear combination:

$$H_j(s) = (1 - f_j)H_1(s) + f_j H_2 \qquad (5)$$

where f_j is a disorder parameter. As shown in Figure 7b, the intensities of Peierls peaks are indeed decreased but they stay relatively sharp, indicating that the simplistic model of independent statistics may not be sufficient to model the experimental data fully. Finally, Figure 8 shows an attempt to reproduce semi-quantitatively the experimental scattering curves for SomP at different temperatures using the model having three layer thickness: two organic layers (d_1 = 2.6 nm, i.e. $f_1 = f_2 = 0$ which represents the stack with the long organic layer thickness; d_1 = 2.2 nm, i.e. $f_1 = f_2 = 1.0$ which represents the stack with the short organic layer thickness) with thickness distributions ($\sigma_1 = \sigma_2 = 0.15$ nm), and one mineral layer that can be described via the form factor. Clearly, all the observed peaks can be accounted for and the original chaos of these scattering curves has essentially been resolved into a consistent model with very few parameters. The parameters used for the

Table 1. Model parameters used in calculating the scattering profiles in Fig. 8. Each profile was calculated based on three types of stack with a volume fraction w_i (i = 1, 2, 3; $w_1 + w_2 + w_3$ = 1). The disorder parameters $f_1(w_i)$ and $f_2(w_i)$ characterize the periodicity of stacks; $f_1 = f_2 = 0.0$ represents an AA-type stack formed by lamellae with d_1 = 2.6 nm and σ_2 = 0.15 nm; $f_1 = f_2 = 1.0$ represents a BB-type stack formed by lamellae with d_1 = 2.2 nm and σ_2 = 0.15 nm; f_1 = 0.1 and f_2 = 0.9 represents an imperfect Peierls stack.

T (ºC)	w_1	$f_1(w_1), f_2(w_1)$	w_2	$f1(w_2), f_2(w_2)$	w_3	$f_1(w_3), f_2(w_3)$
30	0.25	0.0, 0.0	0.75	0.1, 0.9	0.00	1.0, 1.0
160	0.90	0.0, 0.0	0.05	0.1, 0.9	0.05	1.0, 1.0
280	0.70	0.0, 0.0	0.0	0.1, 0.9	0.30	1.0, 1.0
200 cooled	0.75	0.0, 0.0	0.15	0.1, 0.9	0.20	1.0, 1.0
30 cooled	0.02	0.0, 0.0	0.60	0.1, 0.9	0.38	1.0, 1.0

simulation are listed in Table 1. We note that the perfectly alternating stack has the parameters $f_1 = 0$ and $f_2 = 1$ (or *vice versa*) so the fitted parameters with $f_1 = 0.1$ and $f_2 = 0.9$ indicate that the observed Peierls stack is almost perfectly alternating. The volume fraction for each type of stack is indicated by w_i ($i = 1.3$), $w_1 + w_2 + w_3 = 1$. The temperature dependence of the lamellar structure, involving these three different stack systems, was described earlier. Again we emphasize that these scattering curves could be resolved from the structure point of view. The chemical reasons for the observed structure changes, however, remain unclear and will be the subject of future study.

The SMAE organoclay contained a different surfactant component (DMDTA) than SomP (HTBP) and thus exhibited different scattering profiles (Figure 5b) and different lamellar structure changes upon heating. However, the two-organoclay systems still shared some common structure traits as well as thermal behavior. For example, at 30ºC, the first-order maximum in SMAE (Figure 5b) was found to contain two peaks centered at 0.28 and 0.33 nm^{-1}, respectively. Similar splitting of a second-order maximum (at 0.32 and 0.64 nm^{-1}) suggests the presence of at least two independent lamellar systems: α ($s_{1\alpha} = 0.28$ nm^{-1}) and β ($s_{1\beta} = 0.32$ nm^{-1}). The presence of a weak peak at 0.16 nm^{-1} indicates the Peierls distortion in the β lamellar system. The thermally induced peak splitting was much less pronounced in SMAE than in SomP. At 50ºC, the Peierls peak disappeared and the two split first-order peaks merged into a sharp symmetric peak having a Lorentzian characteristics (the peak is centered at $s = 0.3$ nm^{-1}). With the increase in temperature, the first-order SAXS peak shifted towards a lower s value (*e.g.* at 260ºC, the peak is centered at $s = 0.26$ nm^{-1}). Components of the asymmetric second-order SAXS peak, initially centered at 0.6 nm^{-1}, also gradually merged as temperature increased. At 180ºC, the second-order peak became symmetric and was positioned at the s value exactly twice the position of first-order peak, indicative of a unimodal layer thickness distribution. As temperature increases to 280ºC, the SAXS peaks became weaker and no longer equidistant, with $s_2 > 2*s_1$, indicating that some organic layers were collapsed due to thermal degradation of DMDHDA. Similar structure changes (*i.e.* the weakening of scattering signals and the re-occurrence of non-equidistant peak positions) have also been observed in the montmorillonite-DMDHDA system (Gelfer *et al.*, 2004). As temperature decreased from 280ºC to 30ºC, the SAXS maxima became broader and shifted towards greater s values, indicating the decrease in the long spacing, which was consistent with the surfactant loss. The Peierls peaks could not be observed in the scattering profiles from the cooled SMAE samples. It appeared that the surfactant degradation resulted in the loss of AB-type periodicity (the Peierls alternating stack).

At the present time, we can only hypothesize about the structural reasons for the appearance of alternating stacks in 'Somasif' minerals. Based on the abundance of tubular structures seen in SEM (Figure 1), it may be suggested that the 'Somasif' clay is not a complete 2:1 smectite system having octahedral sheets sandwiched between two tetrahedral sheets. In other words, a fraction of the 'Somasif' clay may consist of 1:1 mineral layers with two structurally different tetrahedral (T) and octahedral (O) sheets and thus different surface properties. In this case, it is conceivable that when similar sides (O or T) are facing each other, the OO couple may have different local ion exchange capacity than the TT couple. In addition, the organic layers sandwiched between T sides of the clay layer may have different average thickness and thermal stability than those surrounded by O surfaces. These asymmetric arrangements may lead to the tubular structure.

It has been reported that the naturally occurring 1:1 layer magnesium silicate chrysotile (Panek *et al.*, 2006) with the chemical composition of $Mg_3Si_2O_5(OH)_4$ that is the main component of asbestos, exists predominantly in a tubular structure (*i.e.* the tubular form). We hypothesize that the presence of defects and iso-ionic substitutions within the mineral layers would result in charges on the surfaces of SME100 mineral layers, which can be balanced by exchangeable Na ions located in the interlayer gallery areas. As a result, SME100 can swell in water and exchange Na ions with other cations, which is absent in naturally occurring chrysotile. The size difference between octahedral- and tetrahedral-forming sheets in 1:1 clays thus may be the main driving force for the formation of tubular and rod structures (Giannelis *et al.*, 1999). We further hypothesize that the signficant defects content in SME100 and the prominent presence of exchangeable ions may relieve the stress of the 1:1 layers, so planar structures become as stable as tubular or rod-like structures. Still, the tubular structures are plentiful and notable in 'Somasif'-based materials (Figure 2).

Although the presence of tubular structures and AB-periodicity in SME 100 agree with the 1:1 structure composition, the observed powder WAXD patterns of 'Somasif' are much closer to those known for the 2:1 smectite system (*e.g.* Na-based 'Cloisite') (Figure 9) instead of chrysotile. According to Alexandre and Dubois (2000), 'Somasif' can be synthesized by heating talc with NaSiF$_6$. As the complete transformation from 2:1 mineral (talc) to 1:1 chrysotile-like system is not likely, both 1:1 and 2:1-type components must co-exist. The experimentally observed abundance of the AB-type lamellar structure suggests that the synthetic procedure adopted by Unico results in the formation of chemically different surfaces with charge density and ion exchange capacity being different on alternate sides of the lamellae. However, the present data do not allow us to pinpoint the exact structural reason why charges on different sides of lamellae can promote the formation of tubular structures even in the 2:1 system.
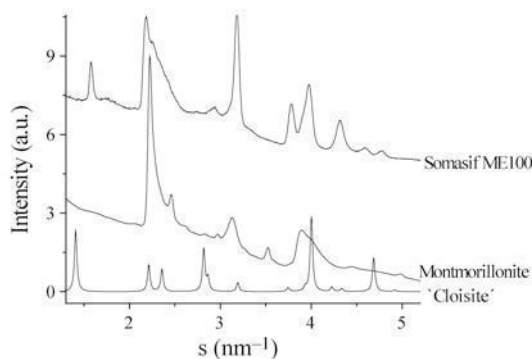
Figure 9. WAXD profiles for 'Somasif' ME100, 'Cloisite' and chrysotile.

Figure 10 illustrates the temperature-resolved WAXD profiles for SomP organoclay. The positions and the shapes of the diffraction peaks in 'Somasif' remained invariant with temperature. The appearance of the small peak at 1.1 nm^{-1} could be attributed to the higher scattering orders of the sharp lamellar signals observed in SAXS. A similar diffraction feature was seen in SMAE (data not shown). These observations suggest that the structural type and the dimension of the mineral layers in 'Somasif' were not strongly affected by the organic modification, supporting our modeling approach to treat the mineral layer as a monolith lamella. In general, the WAXD profiles of SomP organoclay exhibited typical structure characteristics of a layer silicate. The WAXD profiles of organoclays were very similar to those of unmodified SME100, where the observed slight difference could be attributed to a smaller amount of lateral stacking defects present in organoclays.

CONCLUSIONS

Thermal stability and corresponding structure changes of organoclays based on synthetic 'Somasif' minerals were investigated by means of a combination of
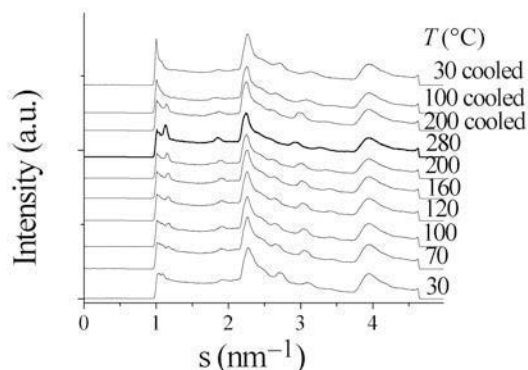
scattering, diffraction, spectroscopic and thermal techniques. The SAXS results indicate that the surface properties of alternating sides of the 'Somasif' mineral layers are different, resulting in 'Peierls-distorted stacks' with AB-type periodicity in the corresponding organoclays. The scattering characteristics of the AB-type periodicity is the low-intensity scattering maximum with its s value corresponding to the combined AB spacing. The temperature-resolved SAXS results indicate that the 'Somasif'-organoclays can be described using a simple model with few structure parameters. The simultaneous occurrence of AB and AA or BB systems manifests itself by the asymmetric shape of the SAXS profile. Heating of 'Somasif'-based organoclays can result in structural rearrangements, causing the shifting and splitting of SAXS peaks as the relative contributions of AA, AB and BB systems would change. It is clear that 'Somasif'-based organoclays consist of two populations of organic layer thicknesses, which can undergo thermal transitions and desorption leading to different lamellar structures. Based on SAXS and SEM results, we also suggest that the 'Somasif' minerals may contain a notable amount of 1:1 clay, some of it in the form of a tubular structure, similar to that of chrysotile (the main component of asbestos). On the other hand, the WAXD data do not seem to contain a significant amount of chrysotile-like structures and are more consistent with the smectite-like structure. Thus, the formation of tubular structures and AB periodicity may be attributed to a 2:1 structure with different charges on alternating sides of mineral layers.

REFERENCES

Alexander, L.E. (1969) *X-ray Diffraction Methods in Polymer Science.* Wiley-Interscience, New York.

Alexandre, M. and Dubois, P. (2000) Polymer-layered silicate nanocomposites: preparation, properties and uses of a new class of materials. *Materials Science and Engineering R: Reports*, **28**, 1–63.

Brindley, G.W. and Brown, G. (1980) Order-Disorder in Clay Mineral Structures. Pp. 125–197 in: *Crystal Structures of Clay Minerals and their X-ray Identification* (G.W. Brindley and G. Brown, editors). Monograph **5**, Mineralogical Society, London.

Chu, B. and Hsiao, B.S. (2001) Small-angle X-ray scattering of polymers. *Chemical Reviews*, **101**, 1727–1761.

Farmer, V.C. (1974) *The Infrared Spectra of Minerals.* Monograph **4**, Mineralogical Society, London, 539 pp.

Gates, W.P. (2004) Crystalline swelling of organo-modified clays in ethanol-water solutions. *Applied Clay Science*, **27**, 1–12.

Gelfer, M., Burger, C., Fadeev, A., Sics, I., Chu, B., Hsiao, B.S., Heintz, A., Kojo, K., Hsu, S.-L., Si, M. and Rafailovich, M. (2004) Thermally induced phase transitions and morphological changes in organoclays. *Langmuir*, **20**, 3746–3758.

Figure 10. Temperature-resolved WAXD profiles for SomP organoclay.

Gelfer, M.Y., Burger, C., Chu, B., Hsiao, B.S., Drozdov, A.D., Si, M., Rafailovich, M., Sauer, B.B. and Gilman, J.W. (2005) Relationships between structure and rheology in model nanocomposites of ethylene-vinyl-based copolymers and organoclays *Macromolecules*, **38**, 3765−3775.

Giannelis, E.P., Krishnamoorti, R. and Manias, E. (1999) Polymer-silicate nanocomposites: model systems for confined polymers and polymer brushes. *Advanced Polymer Science*, **138**, 107−147.

Hackett, E., Manias, E. and Giannelis, E.P. (1998) Molecular dynamics simulations of organically modified layered silicates. *Journal of Chemical Physics*, **108**, 7410−7415.

Hair, M.L. (1967) *IR spectroscopy in Surface Chemistry*. Marcel Dekker, New York.

Hosemann, R. and Bagchi, S. N. (1962) *Direct Analysis of Diffraction by Matter*. North Holland Publishing Co., Amsterdam, The Netherlands.

Ijdo, W.L. and Pinnavaia, T.J. (1998) Staging of organic and inorganic gallery cations in layered silicate heterostructures. *Journal of Solid State Chemistry*, **139**, 281−289.

Ijdo, W.L. and Pinnavaia, T.J. (1999) Solid solution formation in amphiphilic organic-inorganic clay heterostructures. *Chemistry of Materials*, **11**, 3227−3231.

Johns, W.D. and Sen Gupta, P.K. (1967) Vermiculite-alkyl ammonium complexes. *American Mineralogist*, **52**, 1706−1724.

Jonas, E.C. and Grim, R.E. (1957) Differential thermal analysis using controlled atmosphere. Pp. 389−403 in: *Differential Thermal Analysis* (R.C. Mackenzie, editor). Monograph 2, Mineralogical Society, London.

Kojo, K., Ge, S., Takahara, A. and Kajiyama, T. (1998) Molecular aggregation state of *n*-octadecyltrichlorosilane monolayer prepared at an air/water interface. *Langmuir (Letter)*, **14**, 971−974.

Krishnamoorti, R., Vaia, R.A. and Giannelis, E.P. (1996) Structure and dynamics of polymer-layered silicate Nanocomposites. *Chemistry of Materials*, **8**, 1728−1734.

Lagaly, G. (1986) Interactions of alkylamines with different types of layered Compounds. *Solid State Ionics*, **22**, 43−51.

Lagaly, G. (1987) Water and solvents on surfaces bristling with alkyl chains. Pp. 229−240 in: *Interactions of Water in Ionic and Nonionic Hydrates* (H. Kleeberg, editor). Springer, Berlin, Heidelberg, New York.

Lagaly, G., Fitz, S. and Weiss, A. (1975) Kink block structures in clay organic complexes. *Clays and Clay Minerals*, **23**, 45−54.

Lagaly, G., Witter, R. and Sander, H. (1983) Water on hydrophobic surfaces. Pp. 65−77 in: *Adsorption from Solution* (R.H. Ottewill, C.H. Rochester and A.L. Smith, editors). Academic Press, London.

LeBaron, P.C., Wang, Z. and Pinnavaia, T.J. (1999) Polymer-layered silicate nanocomposites: An overview. *Applied Clay Science*, **15**, 11−29.

Lee, J.W., Lim, Y.T. and Park, O.O. (2000) Thermal characteristics of organoclay and their effects upon the formation of polypropylene/organoclay nanocomposites. *Polymer Bulletin*, **45**, 191−198.

Malik, W.U., Srivastava, S.K. and Gupta, D. (1972) Studies on the interaction surfactants with clay minerals. *Clay Minerals*, **9**, 369−382.

Moraru, V. (2001) Structure formation of alkylammonium montmorillonites in organic media. *Applied Clay Science*, **19**, 11−26.

Panek, G., Schleidt, S., Mao, Q., Wolkenhauer, M., Spiess, H.W. and Jeschke, G. (2006) Heterogeneity of the surfactant layer in organically modified silicates and polymer/layered silicate composites. *Macromolecules*, **39**, 2191−2200.

Parikh, A.N., Liedberg, B., Atre, S.V., Ho, M. and Allara, D.L. (1995) Correlation of molecular organization and substrate wettability in the self-assembly of n-alkylsiloxane monolayers. *Journal of Physical Chemistry*, **99**, 9996−10008.

Porter, M.D., Bright, T.B., Allara, D.L. and Chidsey, C.E.D. (1987) Structural characterization of n-alkyl thiol monolayers on gold by optical ellipsometry, infrared spectroscopy, and electrochemistry. *Journal of American Chemical Society*, **109**, 3559−3568.

Reynolds, R.C. (1980) Interstratified clay minerals. Pp. 249−305 in: *Crystal Structures of Clay Minerals and their X-ray Identification* (G.W. Brindley and G. Brown, editors). Monograph **5**, Mineralogical Society, London.

Snyder, R.G., Strauss, H.L. and Elliger, C.A. (1982) Carbon-hydrogen stretching modes and the structure of n-alkyl chains. 1. Long, disordered chains. *Journal of Physical Chemistry*, **86**, 5145−5150.

Tateyama, H., Nishimura, S., Tsunematsu, K., Jinnai, K., Adachi, Y. and Kimura, M. (1992) Synthesis of expandable fluorine mica from talc. *Clays and Clay Minerals*, **40**, 180−185.

Vaia, R.A. and Giannelis, E.P. (1997) Polymer melt intercalation in organically-modified layered silicates: model predictions and experiment. *Macromolecules*, **30**, 8000−8009.

Vaia, R.A., Teukolsky, R.K. and Giannelis, E.P. (1994) Interlayer structure and molecular environment of alkylammonium layered silicates. *Chemistry of Materials*, **6**, 1017−1022.

Walker, G.F. (1967) Interaction of n-alkylammonium ion with mica-type layer lattices. *Clay Minerals*, **7**, 129−143.

Xie, W., Gao, Z.M., Pan, W.P., Hunter, D., Singh, A. and Vaia, R. (2001) Thermal degradation chemistry of alkyl quaternary ammonium montmorillonite. *Chemistry of Materials*, **13**, 2979−2990.